60GHz Channel Characterization using a Scatterer Mapping Technique

A. Papió[*], A. Grau[+], J. Balcells[#], J. Romeu[#], L. Jofre[#], F. De Flaviis[*]

[*]*Electrical Engineering and Computer Sciences Dept., University of California Irvine (UCI)*

Room 2233 Engineering Gateway, UCI, 92697-7625 Irvine, CA, USA

apapioto@uci.edu, franco@uci.edu

[#] *Signal Theory and Communications Department, Technical University of Catalonia (UPC)*

Campus Nord D3-210, Jordi Girona 1-3, 08034 Barcelona, Spain

jofre@tsc.upc.es

[+]*Broadcom Corporation*

5300 California Ave., Irvine, CA 92617, USA

***Abstract*—In this paper, a Scatterer Mapping Technique based on a Multi-Frequency Bi-focusing operator with good imaging capabilities is used to characterize the 60GHz wireless channel in an office environment. The measurement data is also processed to extract the effective number of communication channels. The relation between the 60GHz office scatterer map and the effective number of communication channels is highlighted.**

I. Introduction

Since the past few years, the telecommunications industry has been driving a growing interest for new wireless applications, such as WPAN. As a result, there is a strong interest in having a good understanding of the propagation characteristics of 60GHz wireless indoor channels. More precisely, it is of particular interest to determine the predominance of either a scattering or specular phenomena within the wireless channel. This information is critical to determine whether the 60GHz communications need to be encoded using MIMO diversity techniques (if the channel is rich in scattering) or using beamforming techniques (if a few specular paths are available between the transmitter and the receiver).

The wireless propagation channel may be in general characterized by either the transfer function of the channel [1], or alternatively by a more compact way based on the description of the positions and shape of the main scatterers contributing to the creation of the different wave-paths. The advantages of using one or the other depend on the particular scattering/specular characteristics of the channel. If the channel contains a large number of scatterers/paths, the traditional transfer function may be a more appropriate way to describe it. However, when the number of significant scatterers reduces, the scatterer mapping technique [2] becomes more convenient and intuitive because it allows us to physically identify the location of the scatters within the channel.

In this paper, a 2D Scatterer Mapping technique based on a Multi-Frequency Bi-focusing (MF-BF) operator with good imaging properties is applied to the characterization of the 60GHz channel in a realistic indoor scenario. The proposed real indoor scenario (RIS) is that of an office (RIS-Office-Table) consisting on a rectangular office with a central table, wall covering furniture and two different obstacles (RIS-Office-Laptop and RIS-Office-Wall) separating a T_x and R_x located at both ends of the office as represented in Fig.1. In addition, the effective number of communication channels between the transmitter and the receiver is also extracted by following traditional methods [3] for the characterization of MIMO communication channels. The relation between the two characterization methods is illustrated.

The remainder of the paper is organized as follows. In section II the Scatterer Mapping Technique is presented. Section III provides a description of the measurement system. Section IV presents mapping results of canonical objects at 10GHz and 60GHz for imaging friendly scenarios. The effective number of communication channels for such scenarios is also computed. A relation between both is established. Results for the RIS-Office scenarios are also presented here. Section V is devoted to conclusions.

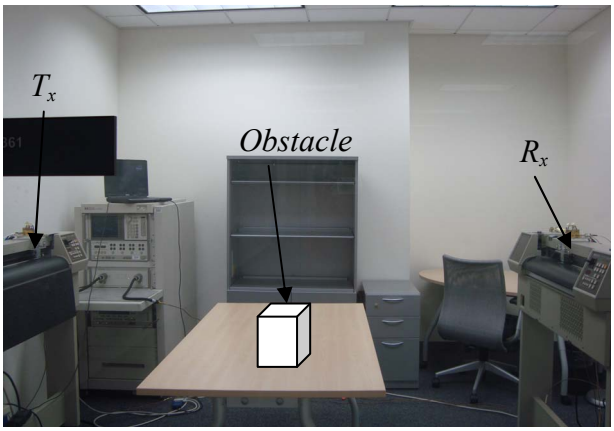

Fig. 1: 60GHz Channel Characterization Geometry.

II. 2D Scatterer Mapping Technique

The general idea for the Scatterer Mapping technique consists on distributing a certain number of microwave

sensors (transmitters and/or receivers) on a certain region, covering as much as possible the area under investigation, as shown in fig. 2. The goal is to obtain the spatial and electrical information of the extended object $\varepsilon_t(\vec{r})$ relative to the original background constant ε_b of the interrogation area S_o. The object can be a continuous distribution or a discrete set of objects S_k with electrical permittivity $\varepsilon_{Sk}(\vec{r})$.

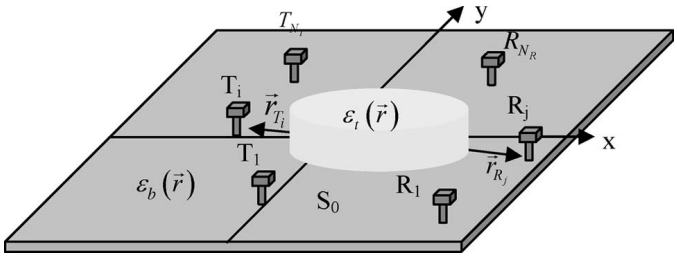

Fig. 2: Scatterer Mapping Technique Sensing Geometry.

In the 2-D geometry, the object is assumed invariant in the z-axis. This allows a scalar formulation of currents and electric fields parallel to the z-axis. Following the electromagnetic compensation principle [4], the illumination by a transmitter located at $\vec{r}_{Ti}$ at a frequency f of an object by a field $E(\vec{r},f,\vec{r}_{Ti})$ induces an equivalent electric current distribution proportional to the electrical contrast $c(\vec{r})=(\varepsilon_t(\vec{r})-\varepsilon_b)/\varepsilon_b$ defined as:

$$J_{eq}(\vec{r},f,\vec{r}_{Ti})=j\omega\varepsilon_b c(\vec{r})E(\vec{r},f,\vec{r}_{Ti}) \quad (1)$$

The induced current at every point of the object as seen in (1) depends for every frequency on both the local contrast value and the value of the illuminating field created by the particular transmitter being active at that moment. This current may be seen as the source of the scattered field in the sensing process and as an illumination-dependent "trace" of the original object in the inverse mapping process.

As shown in Fig. 2, a set of N_T transmitters (T_i) and a set of N_R receivers (R_j) are used to scan the interrogation area where the reconstruction algorithm is applied. First, the information matrix (or channel matrix) is obtained as follows: for every frequency and transmitting element, the scattered field is measured over each receiving element, obtaining an N_R measurement vector. Then, the procedure is repeated for the N_T transmitting elements obtaining an $N_T x N_R$ matrix.

The scattered field measured at a receiver positioned at $\vec{r}_{Ri}$ created by the equivalent current $J_{eq}(\vec{r},f,\vec{r}_{Ti})$ may be expressed as:

$$E_s(\vec{r}_{Ri},f,\vec{r}_{Ti})=-j\omega\mu_0\int_{V_0}J_{eq}(\vec{r},f,\vec{r}_{Ti})G(|\vec{r}_{Ri}-\vec{r}|,f)dV \quad (2)$$

where $G(|\vec{r}_{Ri}-\vec{r}|,f)$ is the Green's function for a 2-D geometry $G(\vec{r})=(1/4j)H_0^{(2)}(kr)$, where $H_0^{(2)}(kr)$ is the second kind zero-order Hankel function and k is the wave number of the background reference medium. For the inverse mapping process based on MF-BF, we may express the "frequency averaged contrast" $\tilde{c}$ as:

$$\tilde{c}(\vec{r})=A_i\sum_{f_{\min}}^{f_{\max}}\sum_{j=1}^{N_R}\sum_{i=1}^{N_T}\frac{E_s(\vec{r}_{Rj},f,\vec{r}_{Ti})}{k^2}\frac{1}{G(|\vec{r}_{Rj}-\vec{r}|,f)}\frac{1}{G(|\vec{r}_{Ti}-\vec{r}|,f)} \quad (3)$$

where A_i is a complex constant including multiple system factors.

The reconstruction algorithm forms every image point of the interrogation area by means of synthesizing two focused groups (bifocusing) of antennas (transmitters and receivers). In (3), the received scattered fields resulting from all the antenna pairs (channel matrix) are numerically weighted by a focusing operator so as to be focused on a unique point of the space under reconstruction. This numerical focusing operator [5] restores the amplitude and phase changes suffered by a wave in its way to and from every scattering point. Applying this focusing operator to the channel matrix for all the points of the image space grid, we are able to obtain a replica of the environment. Since there exist nonlinear phenomena, such as multiple or high-contrast scattering and frequency dependence, a continuous frequency superposition of measurements tends to smooth out and reduce their effects.

For 3-D geometries, the object inhomogeneities in the z-axis causes vertical diffraction and depolarization, and a vectorial formulation must be used based on the 3-D Green function.

III. MEASUREMENT SYSTEM

The 60GHz channel matrix of the measured RIS-Office environments is extracted using two virtual arrays placed at both ends of the office as shown in figure 1. In the transmitter side, an up-converter transforms the 9-11GHz signal generated by the VNA to the 61-63GHz frequency band. A 60GHz band open-ended waveguide acting as the transmitting antenna along with the up-converter is mounted on the moving header of a plotter. The plotter is remotely controlled to scan over its length and create a virtual array of N_T transmitting antennas.

A second plotter is used to create a receiving virtual array of N_R open-ended waveguide antennas. The received signal is down-converted to the 9-11GHz range and brought back to the VNA. Additional power sources and circuitry necessary to drive each transceiver have been mounted on separate boards placed behind the plotters for convenience. In figure 3, details of the down-converter system and plotter fixture can be appreciated.

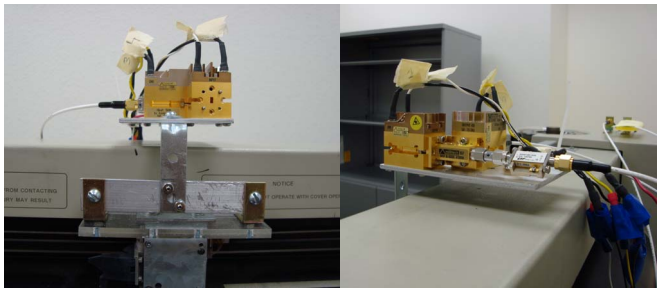

Fig. 3: Plotter fixture holding 60GHz Down-converter.

IV. Results

A. Calibration Results

In this section, a series of short-range measurements for canonical scenarios have been conducted. The aim is to prove the effectiveness of the MF-BF scatterer mapping technique at the 60GHz band compared to that at the 10GHz band, where results have already been presented [6].

It is well known that in the scatterer mapping (or imaging) process, the spatial resolution depends on the operating frequency and the disposition of the sensors on space [6]. Thus, for the sensor disposition of figure 4, a good spatial resolution in the y-axis is expected, while in the x-axis the resolution will be poor, tending to lengthen the objects under analysis. The detection capability depends on the electrical size of the object and the SNR of the system.

In figure 4 we present the 2D scatterer mapping results for measurements conducted over 2GHz bandwidth, at a center frequency of 10GHz. Figure 4a shows the extracted channel mapping when a metallic bar of 15mm diameter was placed where indicated by the blue circle. In the inverse scatterer mapping process, the algorithm is capable to locate the bar on space. Resolution on the x-axis suffers from the aforementioned faults. In figure 4b, 2 metallic bars of 1mm diameter were placed were indicated by the arrow tips. The reconstructed image shows the incapability of the algorithm to detect electrically small objects. This is explained by the fact that the scattered (not reflected) fields by these thin wires are below the noise level or equivalently the RCS (Radar Cross Section) of the object is below the detectable limit for a given SNR (Signal to Noise Ratio).

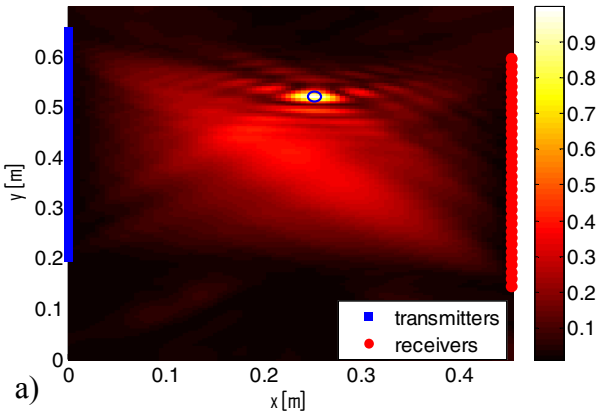

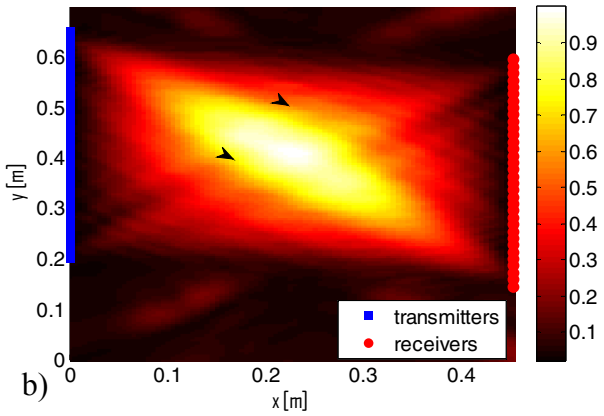

Fig. 4: 10GHz Band Scatterer map of: a) 15mm diameter metallic bar, b) 2 1mm diameter metallic bars.

Figure 5 presents the 2D scatterer mapping results for measurements conducted over 2GHz bandwidth, at a center frequency of 62GHz, for the same scenarios previously presented. In this case, given the increase in frequency, both, the 15mm and the 1mm diameter iron bars can be located in space. This can be explained from the fact that at the 60GHz band the RCS of the object is larger compared to lower frequencies.

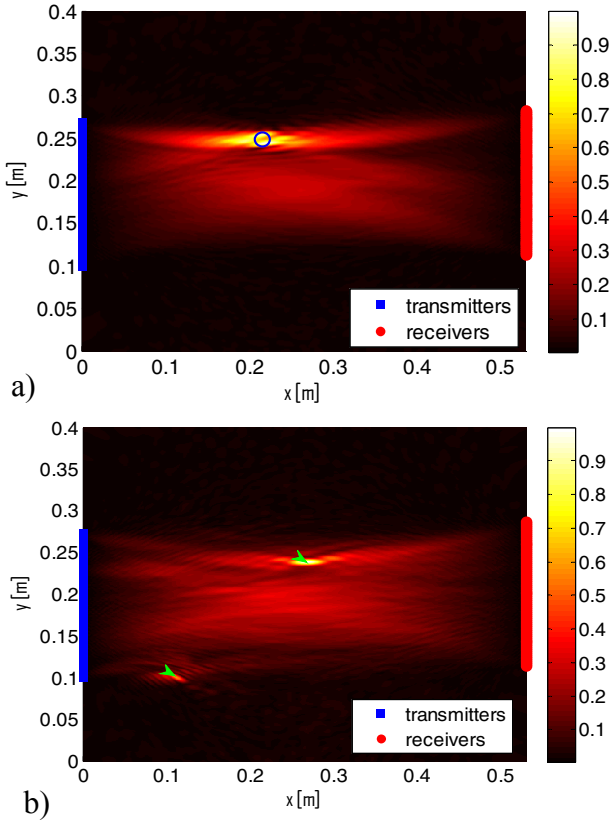

Fig. 5: 60GHz Band Scatterer map of: a) 5mm diameter metallic bar, b) 2 1mm diameter metallic bars.

From the point of view of communication systems, the presence of obstacles in the transmission path between a transmitter and receiver will affect the number of effective

communication channels in a scenario. In an ideal scenario, without fading or multipath, the wireless channel between a transmitter and a receiver has a single effective communication channel, given by the LOS path. In a scenario with Rayleigh fading, the number of effective channels will normally increase with the number of reflecting objects and scatterers. For the sequel, we define the number of effective communication channels as the number of eigenvalues of the channel matrix which are above a critical value (λ_c). To calculate the number of effective channels we have first normalized the channel matrices according to [3]. This normalization allows us to have a more accurate estimation of the diversity order and correlation properties of the channel.

Figure 6 presents the computed effective number of communication channels for the 10GHz scenarios shown in figure 4 with the metallic bars, and comparing it with the empty case (without any metallic bar). It is observed, that in the empty case scenario, the number of effective channels varies from 2 to 3 depending on the frequency. The fact that the number of effective channels is not one (corresponding to the LOS case), indicates that the walls of the room or the metal around the plotters are also contributing to produce multiple replicas of the transmitted signal through reflections. For the 1mm iron bars, the effective number of channels remains unchanged, which agrees well with the fact that in the scatterer mapping of figure 4b the wires were not detected. For the case of the 15mm bar, an appreciable increase in the effective number of communication channels is experienced all over the frequency band. This is an indicative of the presence of a main scatterer in the scenario, that we also verified using the mapping technique, as shown in figure 4a.

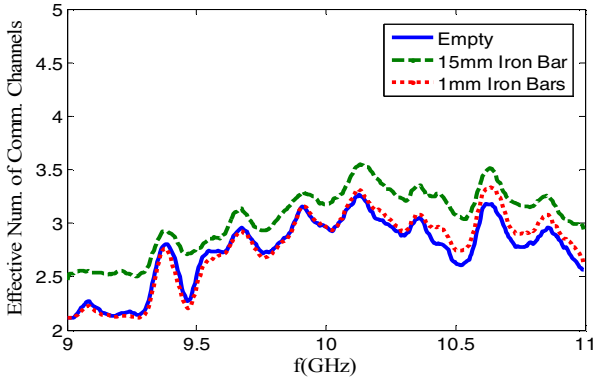

Fig. 6: Effective number of communication channels versus frequency for the scenarios of figure 4 including the empty reconstruction area.

Figure 7 presents the computed effective number of communication channels for the 60GHz band scenarios of figure 5 with the metallic bars and compares them with the case of an empty room. Again, for the empty case, the contributions from the reflections in the walls and plotters are also observed because the number of effective channels is well above one. For the 60GHz measurements, we observe that in both the 1mm and the 15mm wire cases there is an increase in the effective number of communication channels with respect to the empty case. However, the influence varies from one case to the other. Since the 15mm bar is a main scatterer (fig. 5a), the increase in the number of channels is considerably larger in the whole frequency range. The effect of the 1mm wires, however, is still not very significant and should be studied in greater depth.

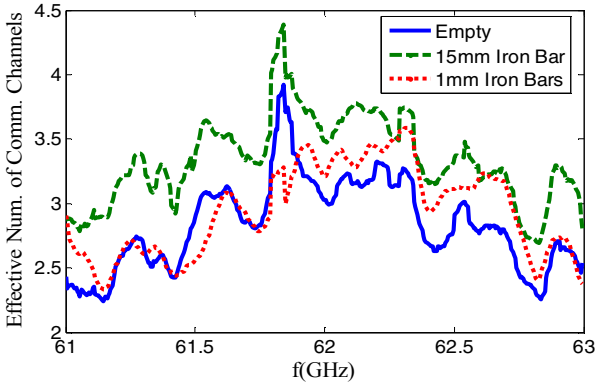

Fig. 7: Effective number of communication channels versus frequency for the scenarios of figure 5 including the empty reconstruction area.

B. *RIS-Office Results*

The scatterer mapping technique is now applied to a real office environment to determine the effect of different objects on the communications channel.

In figure 8 we present the 2D scatterer mapping results for measurements conducted over 2GHz bandwidth, at a central frequency of 62GHz in a RIS-Office environment. Figure 8a (RIS-Office-Laptop) shows the mapping result for the scenario of figure 1, with a laptop located on top of the table (limits marked in green) at the position given by the blue print. The laptop is identified by the algorithm as a huge scattering object extending on the upper half-side of the table.

Figure 8b (RIS-Office-Wall) shows the results of the same scenario removing the laptop and locating a semi-transparent plastic wall close to the table at the position indicated by the blue print. The filled blue squares represent metallic structure supports. In this case, the scattering technique produces a similar result as that on an empty room (except for a second detected object, but weak, on the top of the detection region). This is because the wall effectively is nearly invisible from an electromagnetic point of view.

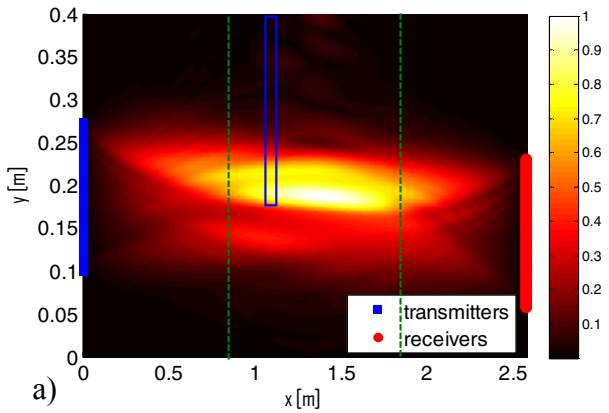

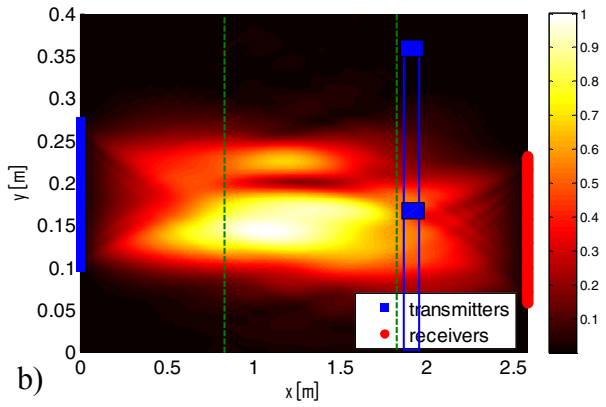

Fig. 8: 60GHz Band Scatterer map of: a) RIS-Office-Laptop, b) RIS-Office-Wall.

In figure 9 the analysis of the effective number of communication channels versus frequency for the cases of figure 8 plus the RIS-Office-Table scenario is presented. It can be observed that due to the multiple reflections from the walls and plotters, the effective number of communication channels for the RIS-Office-Table fluctuates between 3.4 and 4.2 over the frequency range. With the presence of the Laptop, the number of effective channels is increased by close to 1. Given that the laptop acts as a main scatterer, in case that the LOS path between transmitter and receiver was blocked, signal reception would still be possible due to the presence of it. This relates again with the scatterer mapping of figure 8a. With the presence of the wall, the number of effective channels is also increased, but more moderately. This can be explained by the fact that the wall is a non-metallic penetrable-object (nearly electromagnetically invisible), and thus the scattered power is small.

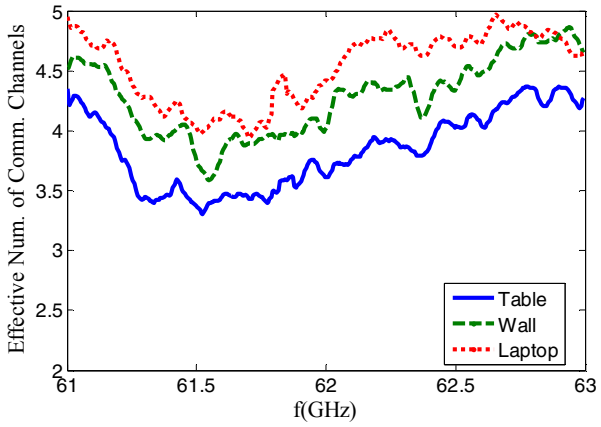

Fig. 9: Effective number of communication channels versus frequency for the scenarios of figure 8 including the empty RIS-Office scenario.

V. Conclusions

In this paper we have proved that a 2D Scatterer mapping technique with good imaging capabilities can be used to effectively characterize a 60GHz wireless communications channel.

A correlation between the scatterer mapping results and the effective number of communication channels in the same scenario has been established.

Canonical scenarios have been measured at both the 10GHz and the 60GHz band. Results confirm the higher resolution of the scatterer mapping technique at the higher frequency band and prove that the scatterer mapping technique is applicable at 60GHz. In addition, measurements at 60 GHz on more realistic office scenarios have been conducted.

Acknowledgment

The authors wish to thank Broadcom Corporation and Intel Corporation for providing technical and financial support to this project.

A. Papió wishes to thank Fundación Caja Madrid, who sponsors her PhD studies through their Post-Graduate fellowship.

References

[1] L. Clavier, M. Rachdi, M. Fryziel, Y. Delignon, V. Le Thuc, C. Garnier, P.A. Rolland, "Wideband 60GHz indoor channel: characterization and statistical modeling," *IEEE Vehicular Technology Conference,* vol. 4, pp. 2098-2102, 7-11 Oct. 2001.

[2] L Jofre, A. Papió, J. M. Jornet, P. Ceballos, J. Romeu, S. Blanch, A. Cardama, "UWB Short-Range Bifocusing Tomographic Imaging," *IEEE Trans on Instrumentation and Measurement,* vol. 57, no. 11, pp. 2414–2420, Nov. 2008.

[3] M. A. Jensen, J. W. Wallace, "A Review of Antennas and Propagation for MIMO Wireless Communications", *IEEE Trans on Antennas and Propagation*, vol. 52, no. 11, pp. 2818-2824, Nov. 2004.

[4] R. F. Harrington, *Time-Harmonic Electromagnetic Fields*, New York: McGraw-Hill, 1961.

[5] Y. J. Kim, L. Jofre, F. De Flaviis, M. Q. Feng, "Microwave reflection tomographic array for damage detection of civil structures", IEEE Trans. on Antennas and Propagation, vol. 51, pp. 3022-3032, Nov. 2003.

[6] L. Jofre, A. Broquetas, J. Romeu, S. Blanch, A. Papió, X. Fabregas, A. Cardama, "UWB Tomographic Radar Imaging of Penetrable and Impenetrable Objects", *Proceedings of the IEEE*, vol. 97, no. 2, February 2009.